

DISLOCATION MODELING OF CREEP-RELATED TILT CHANGES

BY STUART MCHUGH* AND MALCOLM J. S. JOHNSTON

ABSTRACT

Tilt changes associated with 1 to 5 mm of fault creep have been detected at several different locations on the San Andreas fault on tiltmeters within 500 meters of the creep observation point. The creep-related tilts have amplitudes of $\lesssim 0.5 \mu\text{rad}$ and durations comparable to the creep events. No changes $\gtrsim 10^{-2} \mu\text{rad}$ have been observed on tiltmeters at distances $\gtrsim 1$ km from the fault at the time of the creep events. Dislocation models capable of replicating the creep-related tilt events have been constructed to examine the relationship of the model parameters to details of the tilt wave forms. The tilt time histories, source-station configuration, and the displacement time history can be used to infer the type and amount of the displacement, the propagation direction and depth of the slip zone. The shallow depth and finite size of the slip zone indicated by these models contrasts with the horizontal extent over which many creep observations occur. Slip of longer duration and larger extent at depths below a few kilometers that loads the surface material to failure could explain these observations.

INTRODUCTION

The application of dislocation theory to seismology and, in particular, to the mechanics of faulting, provides a mathematical basis for fault models that can quite accurately describe fault failure. One particularly interesting problem concerns aseismic fault failure. When observed at the Earth's surface this is generally termed fault creep (Nason *et al.*, 1974; Yamashita and Burford, 1973). There is practically no detailed knowledge of this process, although it is of fundamental importance to the mechanics of faults such as the San Andreas.

Attempts to answer the question whether the amplitude and time history of fault slip at depth is the same as that observed occasionally at the surface, have only recently become possible. Preliminary results from tiltmeters (Johnston *et al.*, 1976; McHugh and Johnston, 1976; Mortensen *et al.*, 1977) and strainmeters (Jones and Johnston, 1976; Mortensen *et al.*, 1977), installed near sections of the fault where episodic creep occurs, indicate that the near-surface behavior is different from that at depth. This paper concerns, first, a discussion of quasi-static dislocation modeling of episodic surface-creep observations (creep events) that have been simultaneously observed on tiltmeters installed near the San Andreas fault. In particular, the sensitivity of the solution to geometry (length, vertical extent and depth of slip zone, and positions of monitoring stations), spatial and temporal distribution of slip, slip amplitude, and fault-zone properties is discussed. Were sufficient data available a rigorous inversion in terms of these models using the techniques outlined in Jackson (1972) would be possible. Since this is not the case the modeling problem reduces to finding the simplest best-fitting model that satisfies the data. The second part of the paper concerns applying these techniques to data from two specific regions of the San Andreas fault where creep and nearly simultaneous tilt events have been observed.

* Present address: Stanford Research Institute, 333 Ravenswood Avenue, Menlo Park, California 94025

Frank (1973) proposed a model of strike-slip fault creep for which creep events are seen as infinitely long-edge dislocations in a homogeneous semi-infinite half-space. Although some aspects of the observed co-creep tilt and strain observations can be explained with this model, finite models of a vertically oriented rectangular dislocation loop, expanding quasi-statically in an elastic half-space, such as used by Stewart *et al.* (1973), McHugh and Johnston (1976) and Mortensen *et al.* (1977) do appear necessary if the dominant characteristics of the data are to be explained.

INSTRUMENTATION

The creep-related changes in tilt reported in this paper were recorded by biaxial tiltmeters emplaced in shallow (~ 2 m deep) boreholes. These meters operate at a sensitivity of 10^{-8} radians. The amplitude of each tilt component was sampled at 10-sec intervals on an analog chart recorder with a chart speed of 1.26 cm/hr. The creep data from either rod or wire creepmeters were recorded similarly, but with a chart speed of 0.63 cm/hr. Details of the tiltmeter installation are contained in Mortensen and Johnston (1975) and the creepmeter installations are discussed in Yamashita and Burford (1973) and Nason *et al.* (1974).

DATA

The creep-related tilt changes reported previously and also here, occur nearly simultaneously with creep events on the San Andreas fault, 1 to 5 mm in amplitude. The observations have been obtained only on tiltmeters and strainmeters within 0.6 km of the fault. The maximum change in tilt amplitude is typically $< 0.5 \mu\text{rad}$, and the event duration is comparable to the duration of the creep episode. The tilt wave shapes sometimes vary from event to event and from site to site. Often there is a residual tilt associated with these events.

For this discussion data from the tiltmeters MEL, BVY, GVL and LIB and creepmeters XPR1, XMR1, MRC, MRB, MRR and MRW were selected. The locations of these instruments is shown in Figure 1. The creep events and the tilt records for the 12 hr spanning the creep event were digitized from the original records and computer processed to a uniform amplitude scale and a common time scale.

Several examples of simultaneous tilt and creep data from the southern array (MEL, BVY, XMR1, MRC, MRB, MRR and MRW in Figure 1) have been reported by Johnston *et al.* (1976). For each creep event that occurred on any of the creepmeters XMR1, MRC, MRB, MRR or MRW, tilts of between 0.1 to $0.5 \mu\text{rad}$ and with similar form were observed on the tiltmeter MEL. MEL was 0.37 km from the fault. No tilt perturbation greater than $0.01 \mu\text{rad}$ was observed on the tiltmeter BVY at 1.2 km from the fault. Three similar data from the northern array (GVL, LIB and XPR1 in Figure 1), are plotted in Figure 2. Although less complete, the data from the northern array (Figure 2) indicates similar conclusions. Note that the offset in GVL results from the superposition of creep-generated tilts on a diurnal cycle, probably of thermal origin. This signal was subtracted from the record before modeling was attempted, as shown in Figure 9.

An important difference between the northern (GVL events) and southern (MEL events) data is the uniquely different tilt wave form for each of the northern events and the similarity in wave shape for each of the southern events. Although the MEL events are probably caused by similar spatial and temporal slip distributions, nearly identical surface creep events at XPR1 apparently result from more complex and variable displacement distributions as reflected in the GVL tilt. The available tilt

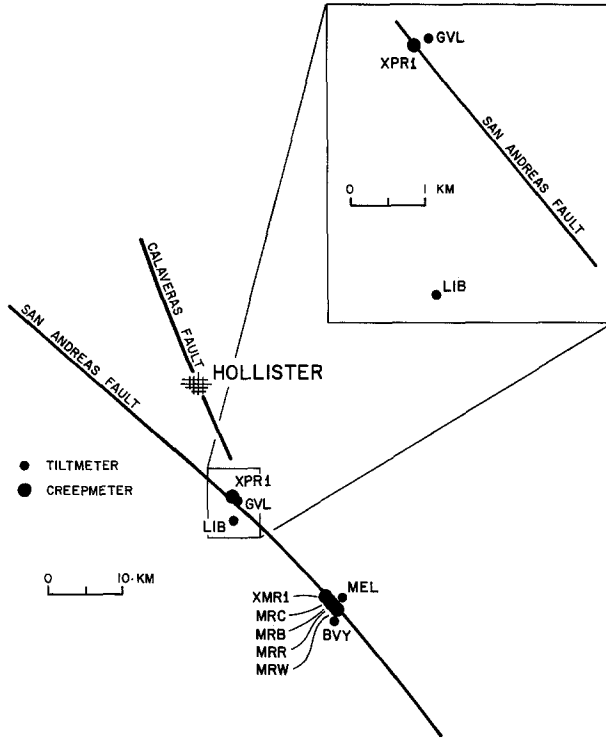


Fig. 1. Location of instruments used in this investigation.

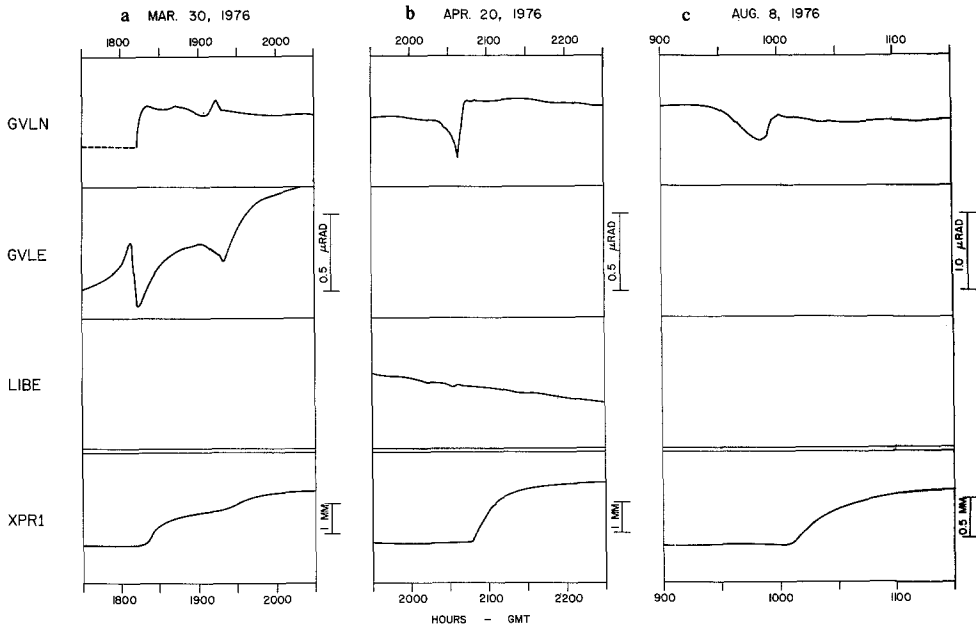


Fig. 2. Three examples of approximately 3 hr of simultaneous records from creepmeter XPR1 and tiltmeters GVL and LIB during creep events on: (a) March 30, 1976, (b) April 20, 1976, and (c) August 8, 1976. GVLE, LIBE and GVLN are the east and north components, respectively. Absence of data indicates an instrument malfunction. Note that the offset at GVLE results from the superposition of creep-generated tilts on a diurnal cycle, probably of thermal origin. The signal was subtracted from the record before modeling was attempted, as shown in Figure 9.

data is inadequate for attempting rigorous inversion. The problem of modeling the physical source of the tilt and creep events reduces to finding and exploring the implications of the simplest physically reasonable model satisfying the observations.

MODELING

It will be assumed initially that the observed tilt changes produced by displacement on the San Andreas fault can be represented adequately by the mathematics of crystal dislocation theory and, in particular, the equations of Press (1965) and Rosenman and

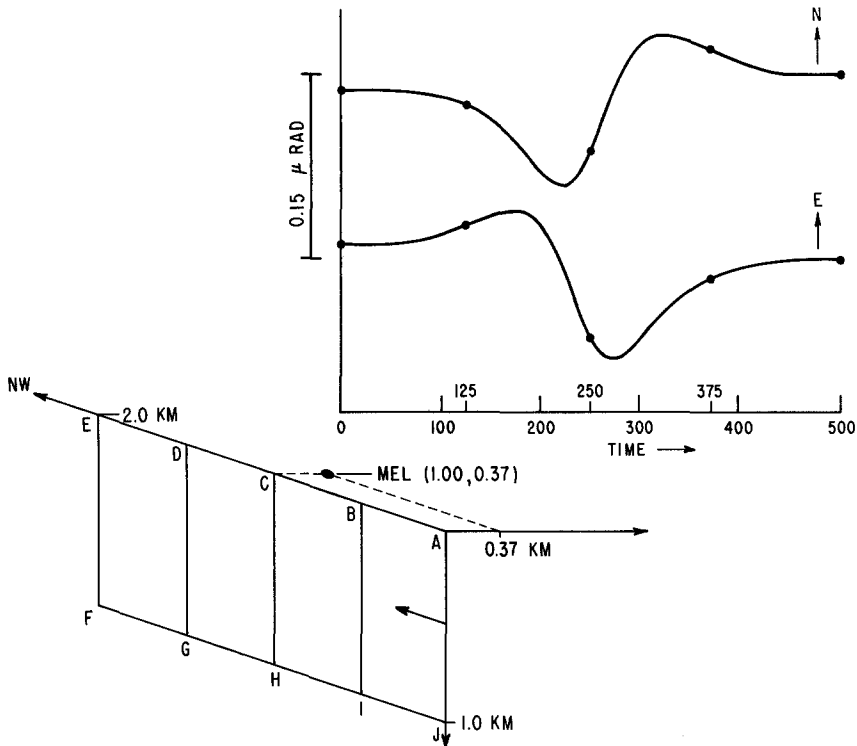


FIG. 3. The slip zone expanding northwest past MEL. Zone expands from position AJ to position AEFJ. The displacement is right-lateral strike-slip incremented from zero to 3 mm in a $(1 - e^{-t/\tau})$ fashion, but is uniform across the slip surface at a given instant. At time $t = 0$, zone is at position AJ, at $t = 125$, zone position is given by rectangle ABIJ; at $t = 250$, slip zone covers rectangle ACHJ; at $t = 375$, ADGJ; at $t = 500$, AEFJ. The tilt wave form is calculated at MEL for this configuration.

Singh (1973). These models utilize a vertically oriented rectangular dislocation loop embedded in an elastic or viscoelastic half-space. Displacement across the slip surface is constant. The resulting surface tilts and strains can then be related to the slip geometry, slip amplitude, and source-station configuration.

King *et al.* (1975) pointed out that since slip propagation velocities are generally small compared with the shear-wave velocity, these models can be used to approximate the tilt time histories by introducing time into the position coordinates, e.g., $x = x_0 - ut$ where u is the component of slip propagation velocity in the x direction. This procedure is mathematically equivalent to calculating the static tilt solution at some observation point for successive increments in source-station position and fault displacement as shown in Figure 3. The rate of change in tilt depends on the fault

displacement rate, the propagation velocity of the slip zone and, in the case of viscoelastic material, the viscoelastic time constant.

It is relatively easy to show for these models that the parameters to which the observed tilt and strain are most sensitive are: (1) the position of the zone boundaries (that is the transition from zero to nonzero displacement relative to the station), and (2) the distribution of fault displacement or slip. In general, both the position of the boundaries and the slip distribution will change with time. Two computer models

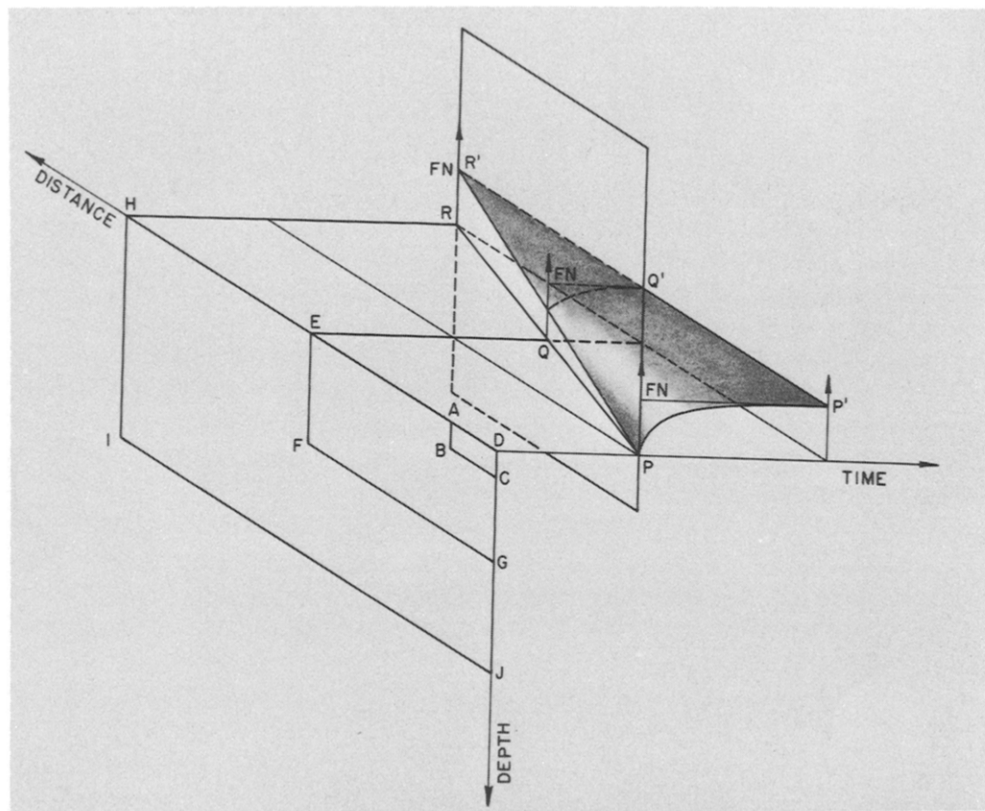
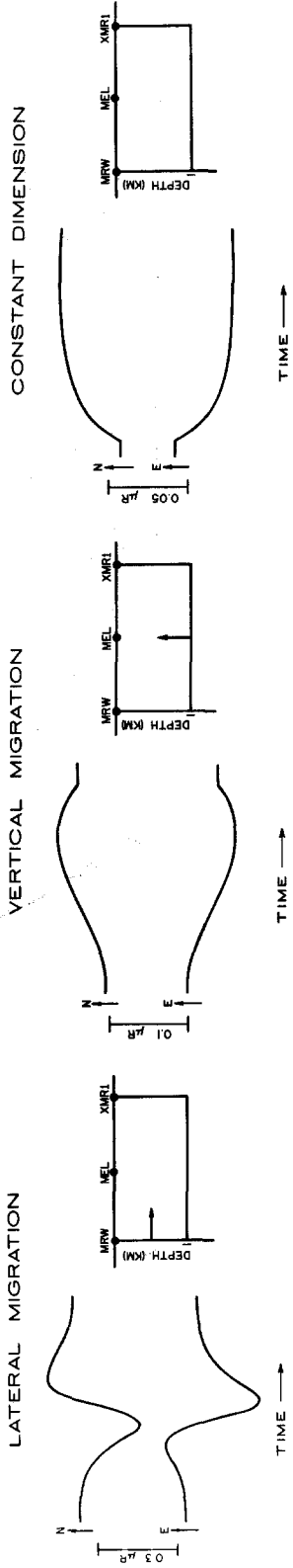


FIG. 4. Details of model I used to generate tilt-versus-time profiles for creep events. A dislocation loop expands from ABCD to HIJD. Corner A moves to position H linearly in time (indicated by line PR). Tilt at a point D results from the entire slip-versus-time profile (PP'). At other points (e.g., E and H) tilt results from only a portion of the complete profile of the displacement with time (QQ' and RR'). FN is the final fault displacement amplitude.

were constructed from the expressions for tilt in Press (1965) that allowed these effects to be examined independently in an elastic half-space. A third model, discussed later, examines the effects expected in a viscoelastic half-space.

The first model (model 1) allows the position of the boundaries to be translated uniformly from some initial to some final position, corresponding to a uniform propagation velocity (McHugh, 1977). The slip is constant over the slip surface for a particular zone, but is allowed to change exponentially with time in the manner indicated by the creep data. Details of this model are shown in Figure 4. If the zone boundaries are fixed, the change in tilt is due solely to the increasing slip with time across the zone. The tilts in this model are less influenced by the form of the slip-time function than by the propagation characteristics of the slip zone (i.e., the changing source-

STRIKE SLIP SOLUTION



DIP SLIP SOLUTION

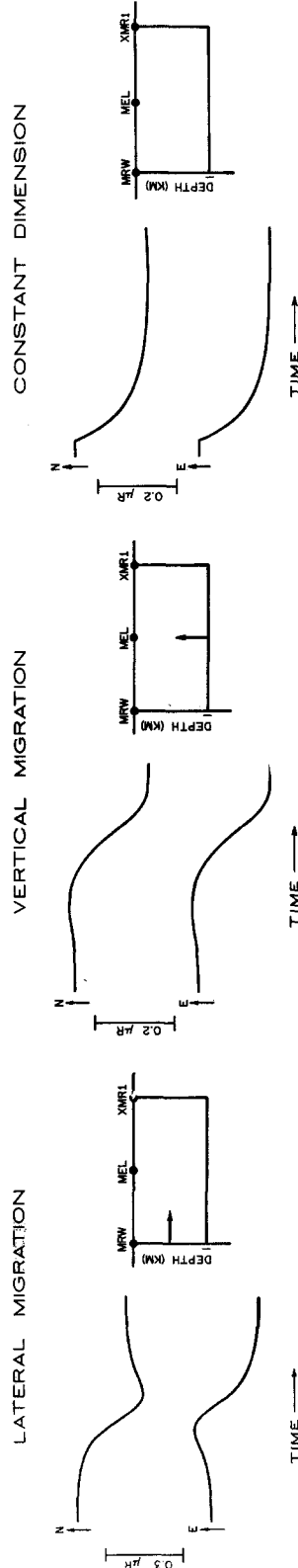


FIG. 5. Examples of tilt wave forms generated by model I for an observation point at MEL and the configuration indicated. The initial configuration is a line at the tail of the arrow. The zone expands in the direction of the arrow. The displacement is incremented from zero to 1 mm with the form $(1 - e^{-t/\tau})$. In the constant dimension case, zone boundaries are stationary, but displacement increases with time.

station configuration). Examples of the basic tilt wave shapes produced by this model are shown in Figure 5.

A more general model (model II) allows the slip distribution function to vary both in space and time. Although it could be argued that introduction of further variables in an already poorly constrained problem is unnecessary, it is instructive to know the relative sensitivity of the solution to reasonable spatial and temporal variations in the slip distribution function. Details of this model are shown in Figure 6.

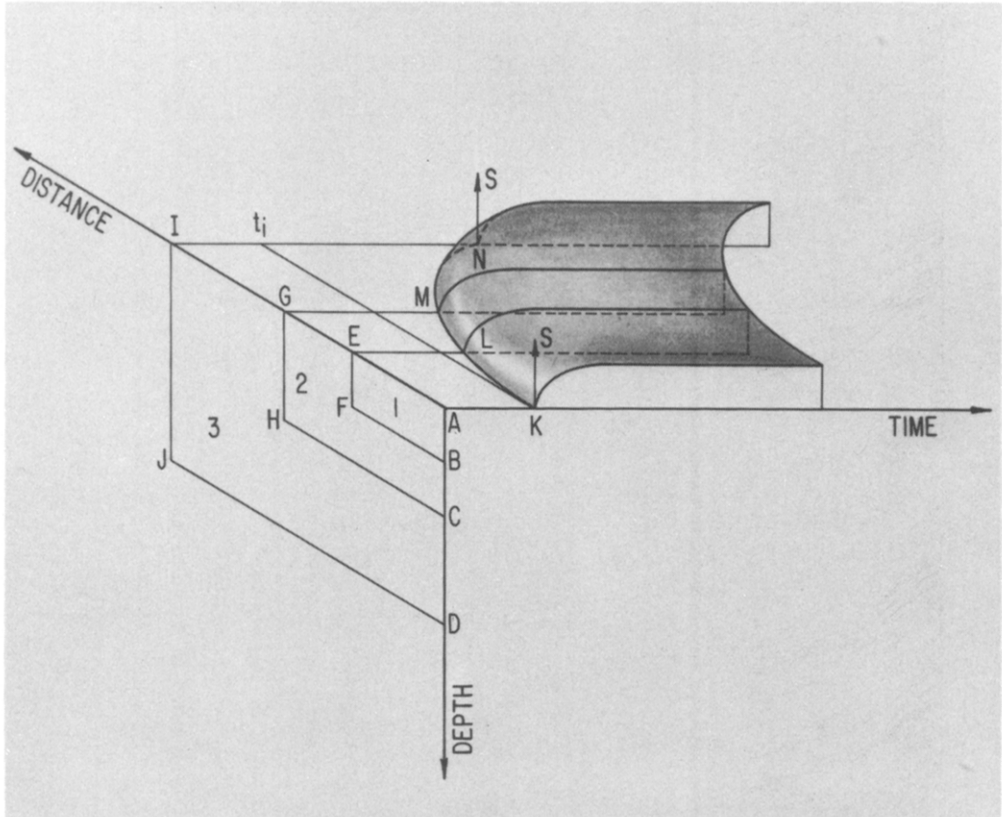


FIG. 6. Details of model II used to generate tilt-versus-time behavior. A dislocation loop expands in distance-depth plane from AEFB1 to AGHC to AIJD. Curve KLMN indicates that the position of the boundary (EF, GH, and IJ) varies exponentially in time (i.e., the creep onset times are distributed exponentially). Curves in the displacement-time plane (S = displacement amplitude) give the slip time history for the dislocation loop at the points indicated. The displacement as a function of position at a given instant can be determined by noting the slip along a constant time line.

Within a particular zone, m , the slip continues to increase from its initial to its final value. If T_j is the total tilt amplitude at a point on the Earth's surface at a time "j" after the initial slip starts propagating and θ_{mn} is the tilt component amplitude for zone m at a time n after the slip is initiated in zone m then, as a consequence of superposition in an elastic medium

$$T_j = \left(\sum_{i=0}^{i=j-1} \theta_{j-i,i+1} \right) - \left(\sum_{i=0}^{i=j-2} \theta_{j-i-1,i+1} \right).$$

In this model the tilts are much more sensitive to the effects of slip rate because the slip is also spatially variable. That is, the amplitude of the slip is greatest where the

zone starts growing, but decays to zero at the zone boundaries. Hence the position of the zone boundaries does not influence the tilt time history as much as they did in model I. Of course, if the slip in model II is constant in time, the slip will be constant in space at each time increment, and the results will be the same as in model I.

It should also be noted that models I and II allow the effects of slip rate to be examined independently of propagation velocity. Because there is an implicit coupling

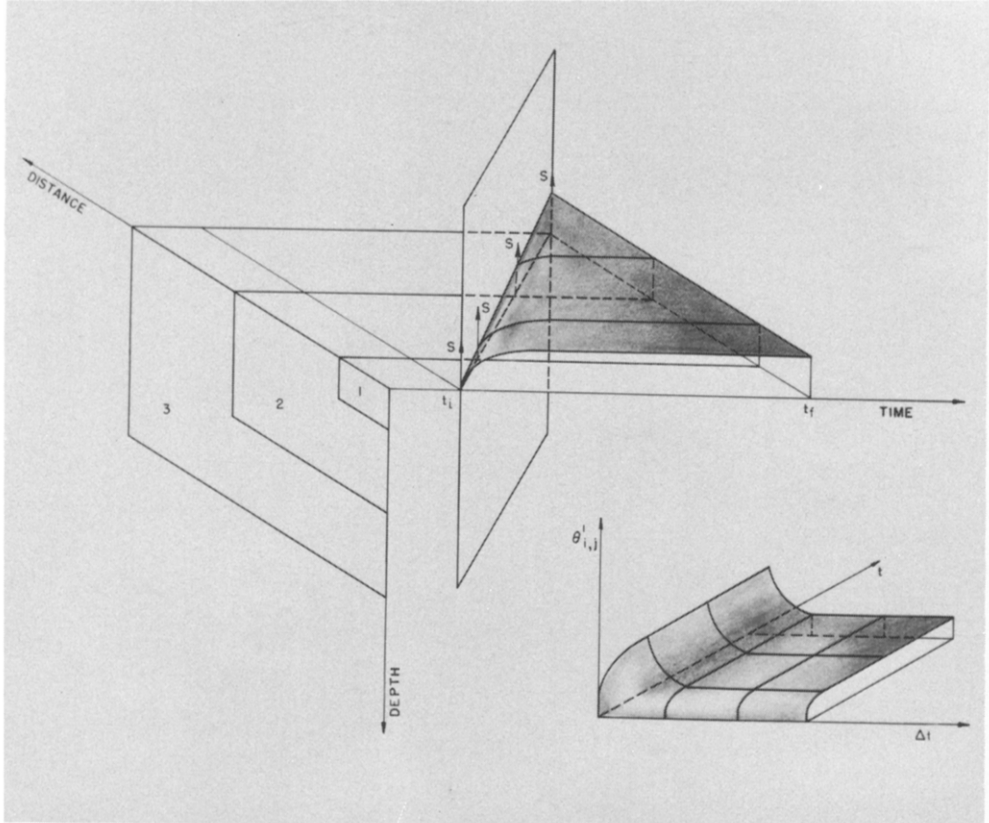


FIG. 7. Geometry used in generating the tilt wave forms in the viscoelastic case. The slip zone expands in the distance-depth plane as indicated, from zone 1 to zone 3. The slip is constant across the zone at a given instant, but changes with time (as indicated by the triangular wedge above the distance-time plane). " S " is the slip magnitude, the initial and final times are indicated by " t_i " and " t_f ", respectively. The *inset* shows the tilt response, $\theta_{i,j}^1$, for an exponentially increasing slip distribution (in the " $\theta_{i,j}^1$ -versus- t " plane) across zone 1. The material response decays exponentially (in the " $t_{i,j}^1$ -versus- Δt " plane) after the initiation of slip.

between the temporal and spatial variation of slip in model II, the tilt wave forms produced by a specific source-station configuration in model I may not be identical to the wave forms produced by model II for the same configuration. For example, the maximum tilt amplitude produced by a specific configuration may be less in model II than in model I because the average slip (i.e., a spatial average) in model II is less than in model I (where the slip is constant over the zone at a given time). Or the maxima and minima in the tilt component amplitude in model II may occur at a later time than in model I (for the same source-station configuration) because the slip at the zone boundaries is initially zero, but increases as the zone grows.

In addition, both models allow strike-slip and dip-slip behavior to be investigated.

The strike-slip and dip-slip zones need not be spatially coincident if they start growing at the same instant. If they are not temporally coincident, one zone may trigger the growth of the other. Therefore various spatial and temporal combinations of strike-slip and dip-slip zone growth may be studied.

The previous discussion has assumed that the half-space is elastic. However, the same procedure may be used for a viscoelastic material. A computer model was introduced that, as before, allows a vertically oriented rectangular dislocation loop, with constant displacement across the loop at a given instant, to be changed in a

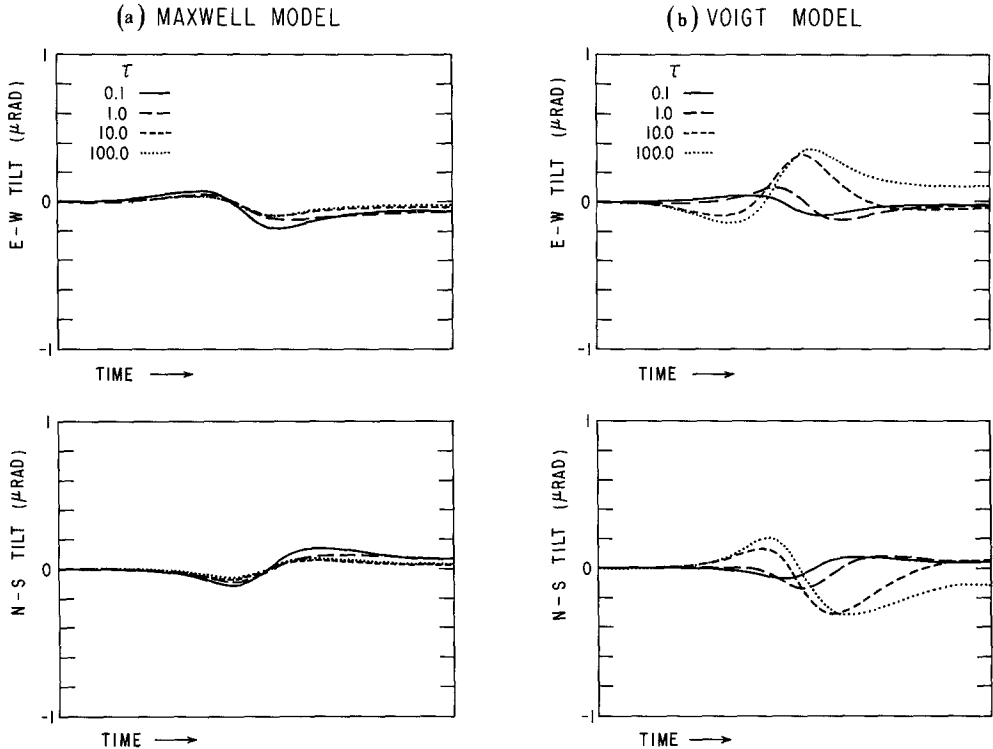


FIG. 8. (a) The theoretical tilt wave forms at MEL generated by laterally propagating strike-slip in a Maxwell viscoelastic material for the configuration in Figure 7. τ is the Maxwell time constant. If $\tau = \text{infinity}$, the Maxwell model reduced to the elastic case (Figure 4). (b) The theoretical tilt wave forms at MEL generated by laterally propagating strike-slip in a Voigt viscoelastic material for the configuration in Figure 7. τ is the Voigt time constant. If $\tau = \text{zero}$, the Voigt model reduced to the elastic case (Figure 4).

quasi-static fashion (Figure 7). The static tilts, for each time increment, are generated from the relations in Roseman and Singh (1973). In effect, this is the viscoelastic analog of model I for the strike-slip case. Examples of wave forms produced by this model are shown in Figure 8. Notice that variations in the Voigt time constant can lead to large departures in tilt amplitude and phase relative to the elastic case.

This group of computer models allows the tilt-time history to be predicted if the source-station configuration, slip amplitude, and viscoelastic time constant are known or can be assumed. To reproduce the observation of the creep-related tilt events discussed previously, it will be assumed that: (1) nonseismic slip can be approximated by the quasi-static incrementing of a rectangular dislocation loop, (2) viscoelastic effects are negligible (i.e., the comparison will be between the elastic model results and the observations), (3) the position of the slip zone producing the creep-related

tilt changes can be inferred from the creepmeter data, (4) the upper boundary of the slip zone coincides with the free surface, and (5) the displacement magnitude across the dislocation loop is approximately the same as the magnitude of the creep event. With these assumptions, either model I or model II can be used to generate the tilt-time history associated with a creep event. By: (1) comparing the predicted to the observed tilt wave forms and (2) using the creepmeter data to constrain the inferred displacement distribution, it should be possible to: (1) determine the relative importance of dip-slip displacement and whether there is any interaction between the strike-slip and dip-slip zones, (2) place bounds on the direction of propagation of the zone (if data from only one creepmeter is available), and (3) infer bounds for the depth of the slip zone.

RESULTS

The observations on the southern array have been discussed elsewhere (Johnston *et al.*, 1976; McHugh and Johnston, 1976) and will not be pursued further here. It is however of interest to discuss the data in Figure 2 and examine the zone geometry and propagation characteristics that can be inferred using both creepmeter and tiltmeter data. Figure 9 illustrates the correspondence between observed and predicted tilt data using model II and some simple source station configurations.

The March 30, 1976 event at GVL appears to be at least partially reproducible using laterally propagating right-lateral strike-slip displacement on the San Andreas fault. If a zone boundary propagates northwest past XPR1 and stops within a few tens of meters of XPR1, the first wave form can be reproduced with 1.5 mm of displacement. The second tilt episode is then initiated by a second creep event (as observed, Figure 2). This second event can be approximated by starting the northernmost boundary of the strike-slip zone used to model the first event, south of XPR1 and allowing this boundary to propagate northwest past XPR1 with the slip increasing from 1.5 to 2.0 mm. If pure strike-slip displacement is used to model the second event, the east-west component predicted at GVL will match the observations quite closely. The north-south component predicted at GVL will, however, increase by 0.4 to 0.5 μ rad. This is not observed (Figure 9).

A fit can be obtained if 0.25 mm of dip-slip displacement (eastside down) is added to the strike-slip displacement as shown in Figure 9. There are unfortunately, no independent data that argue for the existence of such a minor dip-slip component. In any case, the second event does seem to have a more complicated origin than the first. Other models of this event are possible. A sudden acceleration or change in the slip distribution that does not affect the propagation of the boundary can also be invoked to produce a good fit to the data. Minor variations in the amount of dip-slip or changes in the starting and stopping position of the zone may occur without affecting the results. It may be inferred that the propagation velocity of the slip zone near XPR1 and GVL during the first event was fairly uniform because the tilt change is antisymmetric (i.e., an exponential velocity could cause the half-widths of the east-west component maximum and minimum to be quite different).

The April 20, 1976 event at GVL (Figure 9) may be reproduced by 2.2 mm of right-lateral strike-slip displacement propagating laterally, if the vertical zone boundary stops near GVL. Because similar wave forms have been observed on the MEL tiltmeter array associated with a creep event propagating through the array, it was necessary for these MEL events to invoke a combination of dip-slip and strike-slip displacement in which the dip-slip component relaxed after the zone passed the tilt-

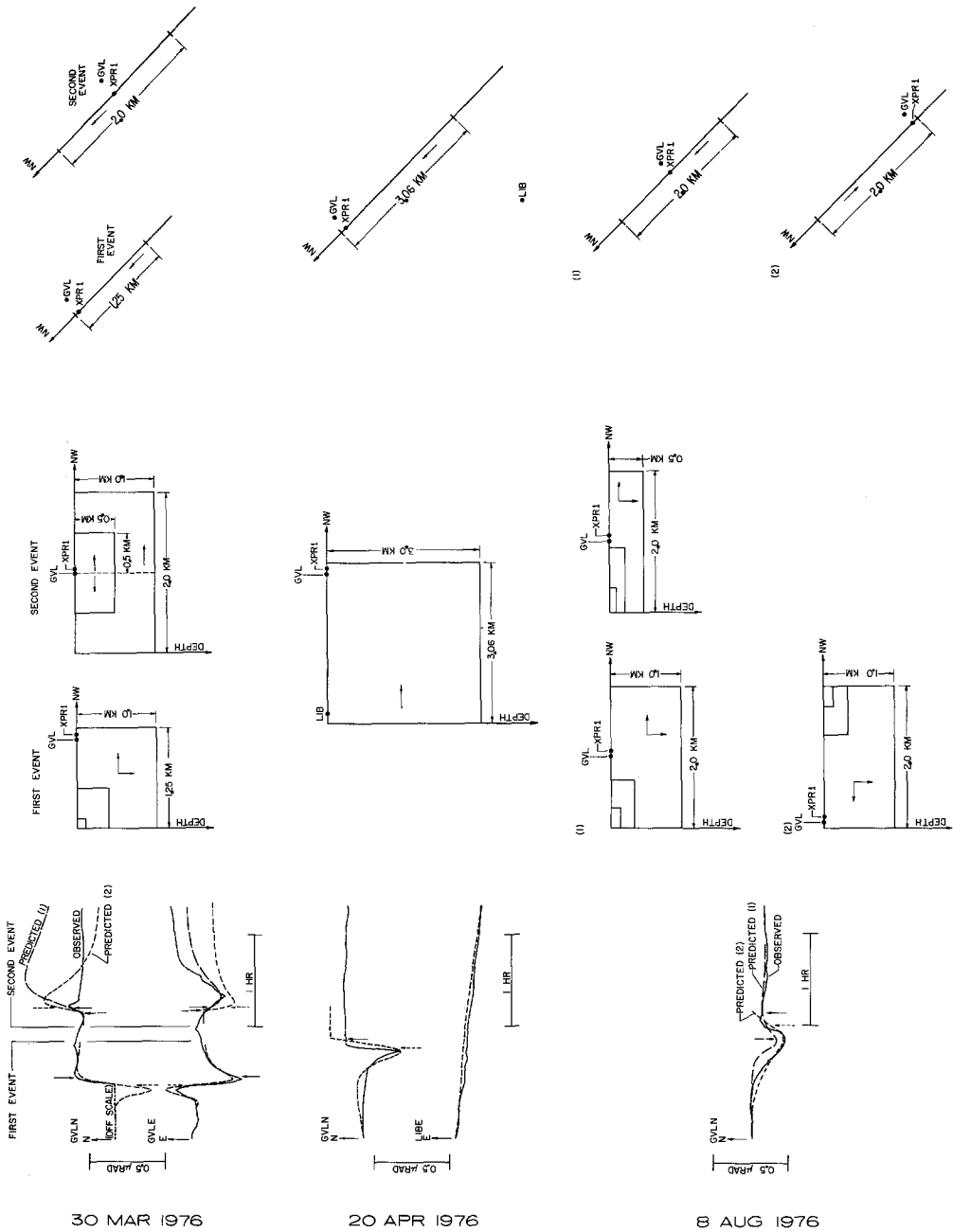


Fig. 9. Comparison of predicted tilt wave forms using model II to those observed at GVL and LIB for events on March 30, 1976, April 20, 1976 and August 8, 1976. The predicted wave forms are indicated by dashed lines and the observed by solid lines. Predicted creep event occurrence times are indicated by dashed arrows and the observed by solid arrows. The first of two events on March 30, 1976 is reproduced with a geometry indicated in columns 2 and 3 by 1.5 mm of right-lateral strike-slip displacement. Other geometries are no doubt possible. The second event is generated (Predicted (1)) by a combination of 1.5 to 2 mm of right-lateral strike-slip and 0.25 mm (east-side down) of dip-slip displacement. The wave form using pure right-lateral strike-slip for the second event is termed Predicted (2). The event on April 20, 1976 can similarly be generated with the simple geometry shown in columns 2 and 3 and 2.2 mm of right-lateral strike-slip displacement. A model (Prediction (1)) requiring 3.5 mm of strike-slip and 0.35 mm of dip-slip displacement can reproduce the event on August 8, 1976. An alternate model (Prediction (2)) of 3.5 mm of right-lateral strike-slip displacement propagating southeast and stopping near GVL can also be fit to the data.

meter (McHugh and Johnston, 1976). Such a model could be used for this event at GVL, in which case the rapid northward rotation might indicate that a dip-slip component relaxed after passage of the creep event. Nevertheless, the simplest model consists of pure right-lateral strike-slip displacement propagating northwestward from LIB and stopping near GVL as indicated.

The August 8, 1976 event (Figure 9) can be reproduced using 3.5 mm of propagating right-lateral strike-slip displacement. Unless nearly 10 per cent dip-slip displacement (east side down) is included in the solution, it is necessary to stop the zone boundary near GVL. Assuming the diurnal component of tilt has been properly removed, the very slight southward rotation between 10.2 and 11.0 hours GMT may be reproduced by including a dip-slip component in the solution, but cannot be re-

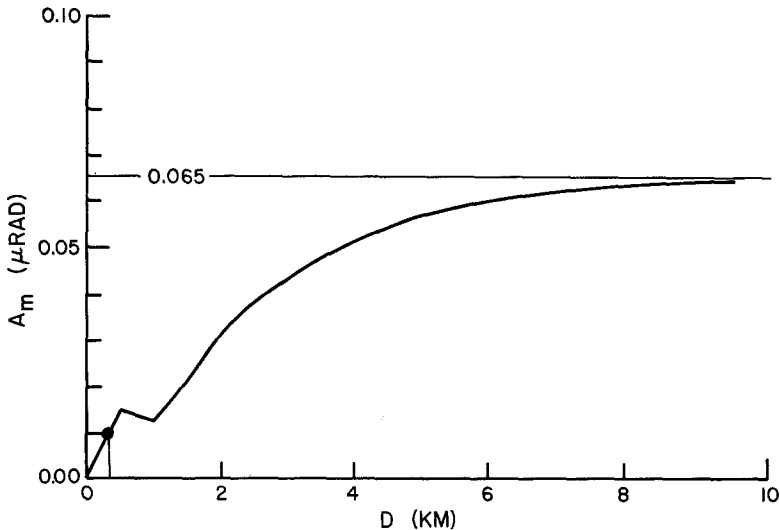


FIG. 10. The maximum tilt amplitude (A_m) at LIB, predicted from the source-station configuration for the April 20, 1976 event in Figure 9, as a function of depth (D) to the lower boundary of the slip zone. $A_m = 10^{-2} \mu\text{rad}$ at $D \cong 0.4 \text{ km}$.

produced with this simple configuration using horizontally propagating pure right-lateral strike-slip displacement.

The previous discussion indicates how the propagation characteristics and the type and amount of displacement may be inferred using the tiltmeter and creepmeter data. The depth of the slip zone at GVL and XPR1 may be estimated from the tilt response of LIB. The lack of a creep-related tilt change $>10^{-2} \mu\text{rad}$ at LIB at the time of an XPR1 creep event suggests either that the slip zone started north of LIB (i.e., is restricted to the GVL-XPR1 area) or that the depth of the slip zone is restricted (assuming that the slip zone propagated past LIB). If it is assumed that slip zone observed at GVL and XPR1 also propagated past LIB, the tilt amplitude at LIB for a specific slip zone model (determined using the GVL-XPR1 data) is a function only of the depth of the slip zone.

Figure 10 illustrates this method for the April 20, 1976 event (the other events will be disregarded because of the complications introduced by LIB being offscale at the time of the creep event at XPR1). The model in Figure 10 (for the April 20, 1976 event) was used to predict the maximum tilt amplitude (A_m) observable at LIB as a function of the depth of the slipping zone (D). If A_m is assumed to be the instrument

resolution (10^{-2} μrad), then D must be less than 1 km, because there was no tilt change $>10^{-2}$ μrad apparent at LIB related to the creep episode at XPR1.

Of course, there are many uncertainties in this estimate of the slip zone depth because the lateral extent of the slip zone is not known and instrumental problems complicate the results. However the discussion does illustrate the kinds of constraints that must be placed on the source-station configuration and the propagation characteristics of the slip zone with these models.

Although instrumental problems obscure the details of the specific slip zone configurations, it is clear that at least some of the creep events cannot be regarded as infinite in extent. Both the lateral dimensions of the zone and its vertical extent must be restricted. This suggests that creep episodes represent fairly rapid failure of the near-surface material probably superimposed on creep of longer duration at greater depths.

As long as the slip propagation velocity remains small compared with the Rayleigh-wave velocity the models discussed previously may be used to predict the tilt change associated with any long-duration displacements at depth. Thus 10 mm of displacement at 5-km depth (representative of the focal depths of many earthquakes in central California) will produce up to 0.03- μrad change in tilt amplitude on surface tiltmeters at 1 km horizontally from the fault, directly above the slipping region. The direction of tilt observed will depend on the position of the tiltmeter. However, the amplitude change will be simultaneous for tiltmeters above the slip zone and its duration will be comparable to the time scale of the displacement change. Thus, if the slip is non-uniform and the related tilts are larger in amplitude than other perturbations in the tilt records, large scale creep at depth should be detectable in near-surface tiltmeter observations. The spectrum of ground noise for these installations indicates that detection at 10^{-8} radians is possible only at periods of a few hours or less. Detection at 10^{-7} radians is possible at periods of about a day and 10^{-6} radians at about a few weeks to a month. Reduction of this spectrum is therefore a most urgent problem if long-term slip propagation is to be detected.

CONCLUSIONS

It has been shown that the main features of the creep-related tilt event data can be reproduced using relatively straightforward dislocation models without violating any of the known physical constraints. The most important constraint is that average slip at depth on the fault be comparable to that observed at the surface. Although classes of models can be fit to the data, there are clearly general restrictions imposed on these classes by the observations. These restrictions involve (1) the size and location of the slipping region, (2) the amount of slip, and (3) the rate of slip. It is apparent that:

(a) The form of the creep-related tilts is not similar to the transient signal expected from a creep wave of infinite extent.

(b) The general features of most of these tilts observed at MEL and GVL can be modeled by right-lateral strike-slip displacement propagating laterally for a distance, generally less than 1 km, along the San Andreas fault. The depth is also apparently less than 1 km. A small component of dip-slip may be required to reproduce some of the details of the tilt wave forms. A more complete data set with better spatial coverage will be necessary for rigorous inversion.

(c) The important and obvious implication of the apparent limited extent and depth of fault displacement detected with the creepmeters XPR1 and XMR1 is

that slip at greater depth is of longer duration and loads the near-surface material to failure.

REFERENCES

- Frank, F. C. (1973). Dislocation models of fault creep processes, *Phil. Trans. Roy. Soc. Ser. A* **274**, 351-354.
- Jackson, D. D. (1972). Interpretation of inaccurate, insufficient and inconsistent data, *Geophys. J.* **28**, 97-109.
- Johnston, J. J. S., S. McHugh, and R. O. Burford (1976). On simultaneous tilt and creep observations on the San Andreas fault, *Nature* **260**, 691-693.
- Jones, A. C. and M. J. S. Johnston (1976). Absence of observable strain at a distance of about 1.5 km from the San Andreas fault during creep events, *Trans. Am. Geophys. Union*, **57**, 1012.
- King, G. C. P., R. G. Bilham, J. W. Cambell, D. P. McKenzie, and M. Niazi (1975). Detection of elastic strainfields caused by fault creep events in Iran, *Nature* **253**, 420-423.
- McHugh, S. (1977). Short period tilt events and episodic slip on the San Andreas fault, *Ph.D. Thesis*, Stanford University, Stanford, California.
- McHugh, S. and M. Johnston (1976). Short period nonseismic tilt perturbations and their relation to episodic slip on the San Andreas fault, *J. Geophys. Res.* **81**, 6341-6346.
- Mortensen, C. E., and M. J. S. Johnston (1975). The nature of surface tilt along 85 km of the San Andreas fault—Preliminary results from a 14-instrument array, *Pure Appl. Geophys. (Milan)*, **113**, 237-249.
- Mortensen, C. E., R. C. Lee, and R. O. Burford (1977). Simultaneous tilt, strain, creep, and water level observations at the Cienega Winery south of Hollister, California, *Bull. Seism. Soc. Am.* **67**, 641-650.
- Nason, R. D., F. R. Philippsborn, and P. A. Yamashita (1974). Catalog of creepmeter measurements in central California from 1968 to 1972, *U.S. Geological Survey, Open File Report* 74-31.
- Press, F. (1965). Displacements, strains, and tilts at teleseismic distances, *J. Geophys. Res.* **70**, 2395-2412.
- Rosenman, M. and S. J. Singh (1973). Quasi-static strains and tilts due to faulting in viscoelastic half-space, *Bull. Seism. Soc. Am.* **63**, 1737-1752.
- Stewart, R. M., C. G. Bufe, and J. H. Pfluke (1973). Creep-caused strain events at Stone Canyon, California, Proc. Conf. Tectonic Problems of the San Andreas fault, *Stanford Univ. Publ., Geol. Sci.*, Stanford, California **13**, 286-292.
- Yamashita, P. A. and R. O. Burford (1973). Catalog of preliminary results from an 18-station creepmeter network along the San Andreas fault system in central California for the time interval June 1969 to June 1973, *U.S. Geological Survey, Open File Report*, Washington, D. C.

NATIONAL CENTER FOR EARTHQUAKE RESEARCH
 U.S. GEOLOGICAL SURVEY
 345 MIDDLEFIELD ROAD
 MENLO PARK, CALIFORNIA 94025

Manuscript received July 29, 1977